Improved oxygen mobility in nanosized mixed-oxide particles synthesized using a simple nanocasting route†

Magali Bonne,[a] Nicolas Bion,[a] Frédéric Pailloux,[b] Sabine Valange,[a] Sébastien Royer,*[a] Jean-Michel Tatibouët[a] and Daniel Duprez[a]

Received (in Cambridge, UK) 22nd May 2008, Accepted 24th June 2008
First published as an Advance Article on the web 1st August 2008
DOI: 10.1039/b808699k

This work reports the synthesis of homogeneously dispersed mixed-oxide nanoparticles (<5 nm) exhibiting improved lattice oxygen mobility (*ca.* two times higher than on bulk samples), using a novel synthesis procedure of nanocasting in mesoporous silica host support.

Since the 1970s, various oxidic phases of perovskite structure (general formula ABO_3) are known to exhibit high activity for gas phase oxidation reactions.[1] Perovskite specific surface areas (SSA) do not exceed a few square meters per gram when prepared by conventional methods such as ceramic routes or coprecipitation. Nevertheless, more sophisticated methods such as complexation,[2a,b] flame hydrolysis,[2c,d] freeze- and spray-drying,[2e] combustion,[2f,g] reactive grinding,[2h,i] microemulsion,[2j]... allow the formation of perovskites with higher SSA (up to 50 $m^2\ g^{-1}$). It is well known that the catalytic activity is strongly related to the SSA of the mixed oxides even if their surface and lattice properties are also suggested to influence the activity.[3] $LnBO_3$ perovskite crystals, where Ln is a lanthanide (generally lanthanum) and B a transition metal (preferably cobalt or manganese), are among the most active oxide materials for gas-phase oxidation.[4] Substitution of A and/or B cation is described as a mean to improve catalytic activity since partial structure substitution resulted in modification of the transition metal reducibility, and consequently of the lattice oxygen reactivity.[5] Indeed, the commonly accepted oxidation mechanism for the CH_4 oxidation reaction involves the participation of lattice oxygen (O^{2-}) *via* a redox cycle on transition-metal active sites (*i.e.* Mars and van Krevelen redox process).[6] Consequently, oxygen mobility in the crystal lattice becomes crucial to obtain high catalytic activity for this reaction. In a previous study, we observed that lattice oxygen mobility was also strongly affected by the crystal domain size (*i.e.* the lower the crystal size is, the higher the lattice oxygen mobility).[7] Decreasing crystal domain size down to values lower than 15–20 nm (by using optimized methods[2c–j]) becomes a real challenge to improve catalytic activity. Hard templating procedures that are described as attractive methods to synthesize high surface area solids,[8] are adequate to control the crystal size growth occurring during crystallization. Consequently, recent academic studies reported the size limited crystallization of perovskite crystals inside hexagonal mesoporous silica support[9] using a conventional citrate gel as precursor. Due to the high viscosity of the citrate complex, the impregnation procedure has to be repeated several times to obtain high precursor loading. Nevertheless, perovskite crystal dispersion inside the silica host support remains one encountered problem. As an example, Nguyen *et al.*[9a] who studied the synthesis of $LaCoO_3$ nanoparticles inside a SBA15-type silica support, noticed "*that their distribution is not very homogeneous in any region of the solid*", and TEM micrographs evidenced crystal segregation on the periphery of the silica particles. Using microwave heating, Yi *et al.*[9b] however obtained more uniform dispersion of ~7 nm $LaCoO_3$ nanoparticles using a similar host support.

We report in this work a novel simple synthesis procedure leading to the formation of embedded mixed-oxide nanoparticles inside a mesoporous HMS-type silica. This synthesis route, based on the self-combustion of metallic precursors with an amino acid is shown to prevent the nanoparticle segregation outside the micrometric silica grains. The oxygen isotopic exchange (OIE) technique is used to evaluate oxygen mobility in the mixed-oxide phase in these novel composites and in reference bulk perovskite samples. Details of the OIE measurements are presented in the ESI.†

A pure siliceous HMS support, synthesized according to the procedure described by Macquarrie *et al.*[10] is used as silica host support. Three perovskites of different compositions ($LaFeO_3$, $LaCoO_3$ and $LaMnO_3$) are synthesized by auto-ignition of the glycinic complex precursors inside the HMS support. Details of the synthesis procedures are provided in the ESI.†

Table 1 summarizes the physical properties of the parent silica support and the supported and reference bulk perovskite samples. A decrease in specific surface area (SSA) is logically observed after the impregnation step, from 832 to 580–620 $m^2\ g^{-1}$ when 15 wt% of mixed-oxide is added. After correction of the surface area to 1 g of host support, the SSA values are found to vary between 591 and 722 $m^2\ g^{-1}$, values slightly lower than that of the silica support, suggesting some pore blocking after impregnation. This assumption was further confirmed by the net decrease in pore volume, as observed for the LaFe-based composites (Fig. 1 and Table 1). Isotherms remain however unchanged (type IV isotherms according to the IUPAC

[a] *Université de Poitiers, LACCO UMR 6503 CNRS, 40, avenue du recteur Pineau, 86022 Poitiers, France. E-mail: sebastien.royer@univ-poitiers.fr; Fax: +33 (0)5.49.45.37.41; Tel: +33 (0)5.49.45.34.79*
[b] *Université de Poitiers, PHYMAT UMR 6630, SP2MI, Boulevard Marie et Pierre Curie, BP 30179-86 962 Futuroscope Chasseneuil, France*

† Electronic supplementary information (ESI) available: Experimental. See DOI: 10.1039/b808699k

Table 1 Physico-chemical properties and activity in oxygen isotopic exchange of supported and bulk perovskites[a]

		Physical characterization				Oxygen isotopic exchange reaction			
Sample	Composition	S_{BET} /m^2 g^{-1}	V_p/cm^3 g^{-1}	D_{BJH}/nm	Crystal phase	$v^\circ_{ex}/10^{19}$ at g^{-1} min^{-1}	$N_{ex}^{60}/10^{20}$ at g^{-1}	O_{ex}^{60} (%)	k_{ex}/ μmolO s^{-1}
HMS	—	832	1.00	3.0	—	0	0	0	0
15LaFe-HMS	13.9wt% $La_{0.97}FeO_3$	622	0.51	3.0	Weak P	5.0	10.8	20	—
25LaFe-HMS	24.5wt% $La_{0.97}FeO_3$	446	0.31	2.9	Weak P	—	—	—	—
15LaCo-HMS	14.2wt% $La_{0.95}CoO_3$	585	0.38	2.8	Weak P	26.3	42.4	77	5.20×10^{-2}
15LaMn-HMS	15.2wt% $La_{0.95}MnO_3$	581	0.40	2.9	Weak P	10.8	34.9	62	2.75×10^{-2}
LaCo	$La_{0.95}CoO_3$	10	—	—	Intense P	138.0	21.1	35	1.81×10^{-2}
LaMn	$La_{0.95}MnO_3$	14	—	—	Intense P	58.0	21.8	31	1.78×10^{-2}

[a] v°_{ex}, initial rate of exchange (defined by eqn (12) in ESI†) evaluated at the beginning of the reaction (first 30 s); N_{ex}^{60}, number of oxygen atoms exchanged at 60 min (defined by eqn (9)–(11) in ESI†); O_{ex}^{60}, fraction of oxygen from the solid exchanged at 60 min. k_{ex}, rate constant calculated from Boreskov' first-order reaction rate (defined by eqn (9)–(11) in ESI†, fitted between 10 and 60 min). Crystal phase: P refers to perovskite phases.

classification,[11] Fig. 1). A long adsorption plateau typical of the N_2 capillary condensation in the mesopores is observed in each case (Fig. 1 and Fig. S1, ESI†). Furthermore, no drastic change in mean pore size, determined by applying the Barrett–Joyner–Halenda model to the desorption branch, can be evidenced (D_{BJH} = 2.5–2.7 nm, Table 1, Fig. S2† for the LaFe-HMS samples).

The small-angle X-ray diffraction pattern (Fig. S3, ESI†) of the HMS support exhibits an intense diffraction peak at 2θ = 2.13°, characteristic of the (100) crystallographic plane of the hexagonal pore structure. Perovskite loaded HMS samples also show a diffraction peak at slightly lower 2θ values (between 1.92 and 2.03°, Fig. S3, ESI†). Peak intensity is found to progressively decrease with the increase of perovskite loading. Such attenuation can be attributed to the progressive pore filling of the silica support (Fig. S3, ESI†).[9a,b] Because of the highly energetic reaction that occurs during glycine combustion, some loss in silica porosity periodicity cannot be excluded.

Weak and broad signals of the different perovskites are detected at high 2θ. No additional peak assigned to the single oxides can be detected (Fig. S4a, ESI†). Furthermore, FWHM of the main peak is larger for the supported perovskites than that obtained on the reference bulk perovskite samples (Fig. S4b, ESI†), indicating a decrease in mean crystal domain size for the HMS based solids. The low signal/noise ratios obtained on the diffractograms for the supported samples (Fig. S4a, ESI†) hinder the use of the Scherrer equation to calculate a mean crystal domain size for these samples. This suggests that the crystal growth is limited by the inorganic walls of the mesoporous silica host support. This conclusion is confirmed by TEM observation where dark contrasts are observed dispersed in the silica particles (15LaFe-HMS, Fig. 2 and S5, ESI†; 15LaMn-HMS, Fig. S6, ESI†). These contrasts are nanometric in size (<5 nm in size), and reveal the presence of a heterogeneous phase. In the thinnest regions of the sample, the magnification can be increased in order to observe the lattice planes of the particles (inset, Fig. 2), which confirms that at least some of these particles are crystallized. The typical contrast of the lattice planes is clearly observed on the corresponding intensity profile (Fig. S7, ESI†), the vertical dotted lines evidencing the edge of the particle (~2 nm). Note that the particle size remains in the same range of order as the mean pore size of the silica (~3 nm, Table 1). Contrarily to what was observed using a citrate gel impregnation procedure,[9a] particles are dispersed evenly inside the micrometric silica particles (Fig. S5 and S6, ESI†). Even if the synthesis procedure used in this work will logically lead to the crystallization of some particles on the external surface of silica, a careful observation of the sample does not reveal external large perovskite crystals. EDXS

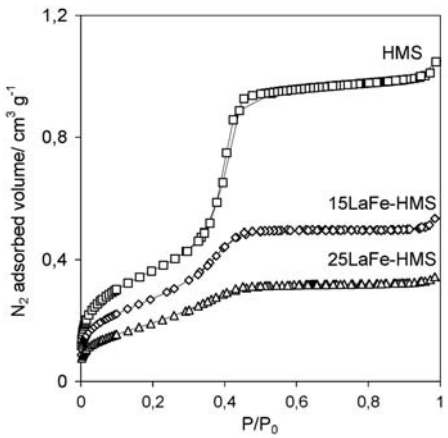

Fig. 1 N_2 adsorption/desorption isotherms at −196 °C obtained for the HMS support and the two $LaFeO_3$ supported samples.

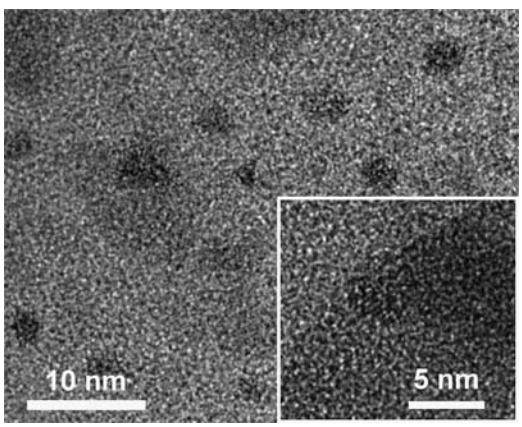

Fig. 2 HRTEM micrograph for the 15LaFe-HMS sample. Inset: Focus on a nanometric crystallized particle.

analysis (Fig. S5 and S6, ESI†) confirms the homogeneous cation dispersion inside the micrometric silica grains. EELS spectra of the Fe-$L_{2,3}$ edge (Fig. S8, ESI†) shows that the dark contrasts observed on the images are probably due to the iron-based nanoparticles. Despite the poor signal to noise ratio, one can observe that the shapes of L_2 and L_3 edges recorded on the 15LaFe-HMS sample are very similar to those recorded on reference samples (bulk $LaFeO_3$ and Fe_2O_3), indicating that the oxidation state of iron is mainly 3+ and that Fe^{3+} ions are located in an octahedral symmetry.[12] This result promotes the idea that the nanoparticles are crystallized. Only slight differences are observed for the 15LaCo-HMS solid (Fig. S9, ESI†). Even if perovskite crystallization did not occur outside the silica grain for this sample, nanoparticle repartition is not homogeneous inside the micrometric grains.

OIE results obtained for selected supported and corresponding bulk perovskites are summarized Table 1. It was first verified that the HMS support does not exhibit any activity in oxygen exchange. Higher initial rate of exchange (v_{ex}^0) is obtained for the bulk perovskites with respect to the supported samples (Table 1, Fig. S10, ESI†). Nevertheless, a careful analysis of the exchange experiments over bulk samples allows to detect small carbon dioxide desorption at the beginning of the exchange test ($C^{16}O_2$ species, Fig. S10, ESI†) that quickly exchanged ($C^{16}O^{18}O$ and $C^{18}O_2$ species, Fig. S11, ESI†). Moreover, the experimental exchange curves do not correlate with the curve shape that would be obtained for a first-order reaction rate with respect to $^{18}O_2$ partial pressure (Fig. S10, ESI†). Such behaviour is not observed for the supported perovskite samples, and the resulting exchange curve shape fits well with a first-order reaction rate. As properly mentioned by Zhang-Steenwinkel,[13] a fast oxygen exchange on surface carbonate species can be supposed to occur over these two bulk samples. Thus, a lower surface carbonate concentration on the supported nanoparticles can be a reason of the low initial rate of exchange. In order to compare bulk and supported samples without carbonate exchange contribution, first-order rate constant (k_{ex}, Table 1) is calculated using experimental values after carbonate exchange (experimental points between 10 and 60 min). Compared to the bulk samples, higher rate constants are obtained for the supported samples (Table 1): 1.6 (LaMn-HMS) and 2.9 (LaCo-HMS). This correlates well with the oxygen exchange capacity measured after 60 min of reaction (O_{ex}^{60}, Table 1). Taking into account the small differences in experimental conditions (catalyst weight, initial $^{18}O_2$ pressure…), the corresponding fraction of oxygen exchanged from the solid at the end of the test are 62 and 77% for LaMn-HMS and LaCo-HMS, respectively, indicating that the supported samples displayed a *ca.* two times higher lattice oxygen mobility (O^{2-} species) than the bulk samples.

Comparison of the three supported samples is presented (Fig. S12, ESI†). The activity order in oxygen exchange is in accordance with that reported by several authors over bulk perovskite for hydrocarbon oxidation reactions.[14]

In summary, the original synthesis procedure reported in this work favours the formation of dispersed mixed-oxide nanoparticles of limited size embedded in a high surface area silica matrix. Evaluation of the supported nanoparticles reactivity by means of oxygen isotopic exchange reaction indicated an improved lattice oxygen mobility than that exhibited by the corresponding bulk samples.

Notes and references

1 (*a*) W. F. Libby, *Science*, 1971, **171**, 499; R. J. H. Voorhoeve, J. P. Remeika, Jr, P. E. Freeland and B. T. Mathias, *Science*, 1972, **177**, 353; (*b*) R. J. H. Voorhoeve, in *Advanced Materials in Catalysis*, ed. J. J. Burton and R. L. Garten, Academic Press, New York, 1977, p. 129.

2 (*a*) P. Courty, H. Ajot, C. Marcilly and B. Delmon, *Powder Technol.*, 1973, **7**, 21; (*b*) M. S. G. Baythoun and F. R. Sale, *J. Mater. Sci.*, 1982, **17**, 2757; (*c*) R. A. M. Giagommuzi, M. Portinari, I. Rossetti and L. Forni, *Stud. Surf. Sci. Catal.*, 2000, **130**, 197; (*d*) R. Leanza, I. Rossetti, L. Fabbrini, C. Oliva and L. Forni, *Appl. Catal., B*, 2000, **28**, 55; (*e*) H. Imai, K. Takami and M. Naito, *Mater. Res. Bull.*, 1984, **19**, 1293; (*f*) V. S. Merzahanov, *J. Mater. Process. Technol.*, 1996, **56**, 222; (*g*) D. Fino, N. Russo, G. Saracco and V. Specchia, *J. Catal.*, 2003, **217**, 367; (*h*) S. Kaliaguine and A. Van Neste, *US Pat.*, US 6,017,504, 2000; (*i*) S. Kaliaguine, A. Van Neste, V. Szabo, J. E. Gallot, M. Bassir and R. Muzychuk, *Appl. Catal., A*, 2001, **209**, 345; (*j*) A. E. Giannakas, A. A. Leontiou, A. K. Ladavos and P. J. Pomonis, *Appl. Catal., A*, 2006, **309**, 254.

3 (*a*) N. Gunasekaran, S. Saddawi and J. J. Carberry, *J. Catal.*, 1996, **159**, 107; (*b*) S. Royer, F. Bérubé and S. Kaliaguine, *Appl. Catal., A*, 2005, **282**, 273; (*c*) G. L. Chiarello, I. Rossetti and L. Forni, *J. Catal.*, 2005, **236**, 251.

4 (*a*) G. Kremenic, J. M. L. Nieto, J. M. D. Tascon and L. G. Tejuca, *J. Chem. Soc., Faraday Trans. 1*, 1985, **81**, 939; (*b*) T. Nitadori, T. Ichiki and M. Misono, *Bull. Chem. Soc. Jpn.*, 1988, **61**, 621.

5 (*a*) S. Ponce, M. A. Pena and J. L. G. Fierro, *Appl. Catal., B*, 2000, **24**, 193; S. Cimino, S. Colonna, S. De Rossi, M. Faticanti, L. Lisi, I. Pettiti and P. Porta, *J. Catal.*, 2002, **205**, 309; (*b*) S. Royer, H. Alamdari, D. Duprez and S. Kaliaguine, *Appl. Catal., B*, 2005, **58**, 273; (*c*) B. P. Barbero, J. Andrade Gamboa and L. E. Cadus, *Appl. Catal., B*, 2006, **65**, 21.

6 M. Stojanovic, C. A. Mims, H. Moudallal, Y. L. Yang and A. J. Jacobson, *J. Catal.*, 1997, **166**, 324.

7 S. Royer, D. Duprez and S. Kaliaguine, *J. Catal.*, 2005, **234**, 364.

8 F. Schuth, *Angew. Chem., Int. Ed.*, 2003, **42**, 3604.

9 (*a*) S. V. Nguyen, V. Szabo, D. Trong On and S. Kaliaguine, *Microporous Mesoporous Mater.*, 2002, **54**, 51; (*b*) N. Yi, Y. Cao, Y. Su, W.-L. Dai, H.-Y. He and K.-N. Fan, *J. Catal.*, 2005, **230**, 249; (*c*) E. V. Makshina, S. V. Sirotin, V. V. Yuschenko, G. N. Mazo, M. W. E. van den Berg, K. V. Klement'ev, W. Grunert and B. V. Romanovskii, *Kinet. Catal.*, 2006, **47**, 49; (*d*) E. V. Makshina, S. V. Sirotin, M. W. E. van den Berg, K. V. Klementiev, V. V. Yuschenko, G. N. Mazo, W. Grunert and B. V. Romanovsky, *Appl. Catal., A*, 2006, **312**, 59.

10 D. J. Macquarrie, D. B. Jackson, J. E. G. Mdoe and H. J. Clark, *New J. Chem.*, 1999, **23**, 539.

11 F. Rouquerol, J. Rouquerol and K. Sing, *Adsorption by Powders and Porous Solids*, Academic Press, London, UK, 1999.

12 L. Garvie and P. Buseck, *Nature*, 1998, **396**, 667.

13 Y. Zhang-Steenwinkel, L. M. van der Zande, H. L. Castricum and A. Bliek, *Appl. Catal., B*, 2004, **54**, 93.

14 (*a*) H. Arai, T. Yamada, K. Eguchi and T. Seiyama, *Appl. Catal.*, 1986, **26**, 265; (*b*) G. Kremenic, J. M. L. Nieto, J. M. D. Tascon and L. G. Tejuca, *J. Chem. Soc., Faraday Trans. 2*, 1985, **81**, 939; (*c*) T. Nitadori, T. Ichiki and M. Misono, *Bull. Chem. Soc. Jpn.*, 1988, **61**, 621; (*d*) D. D. Agarwal and H. S. Goswami, *React. Kinet. Catal. Lett.*, 1994, **53**, 441.

